

Article

TiO₂-Acetylacetonone as an Efficient Source of Superoxide Radicals under Reduced Power Visible Light: Photocatalytic Degradation of Chlorophenol and Tetracycline

Lucas A. Almeida , Anja Dosen, Juliana Viol and Bojan A. Marinkovic * 

Department of Chemical and Materials Engineering, Pontifical Catholic University of Rio de Janeiro (PUC-Rio), Rio de Janeiro 22453-900, Brazil; lucasalmeida@aluno.puc-rio.br (L.A.A.); adosen@puc-rio.br (A.D.); juliana-viol@puc-rio.br (J.V.)

* Correspondence: bojan@puc-rio.br

Abstract: Visible light-sensitive TiO₂-based nanomaterials are widely investigated for photocatalytic applications under high power (≥ 300 W) UV and visible light. The formation of charge transfer complexes (CTCs) between bidentate ligands and nanocrystalline TiO₂ promotes visible light absorption and constitutes a promising alternative for environmental remediation under reduced visible light power. However, the efficiency of photodegradation, the volatilization profile of bidentates, and the role of reactive oxidizing species (ROS) are not fully understood. In this study, thermogravimetric analyses coupled with mass spectroscopy (TGA-MS) were performed on TiO₂-Acetylacetonone (ACAC) CTC. TiO₂-ACAC CTC calcined at 300 °C (TiO₂-A300) was applied for the photocatalytic degradation of chlorophenol (4-CP) and tetracycline (TC) under low power visible light (26 W). Furthermore, the ROS scavengers isopropanol and benzoquinone were added for studying the photocatalytic role of $\bullet\text{OH}$ and $\bullet\text{O}_2^-$ radicals. The TGA-MS showed the release of ACAC fragments, such as ethyl ions and acetone, in the range between 150 °C and 265 °C, while between 300 °C and 450 °C only CO₂ and H₂O were released during oxidation of ACAC. The photocatalytic abatement of tetracycline (68.6%), performed by TiO₂-A300, was ~two times higher than that observed for chlorophenol (31.3%) after 6 h, indicating a distinct participation of ROS in the degradation of these pollutants. The addition of the ROS scavenger revealed $\bullet\text{O}_2^-$ radicals as primarily responsible for the high efficiency of TiO₂-ACAC CTC under reduced visible light. On the other hand, the $\bullet\text{OH}$ radicals are not efficiently generated in the CTC. Therefore, the development of heterostructures based on TiO₂-ACAC CTC can increase the generation of ROS through coupling with semiconductors capable of generating $\bullet\text{OH}$ under visible light.

Keywords: ligand-to-metal charge transfer; anatase; oxygen-based bidentate diketone; sol-gel; TGA-MS; remediation of aqueous pollutants



Citation: Almeida, L.A.; Dosen, A.; Viol, J.; Marinkovic, B.A. TiO₂-Acetylacetonone as an Efficient Source of Superoxide Radicals under Reduced Power Visible Light: Photocatalytic Degradation of Chlorophenol and Tetracycline. *Catalysts* **2022**, *12*, 116. <https://doi.org/10.3390/catal12020116>

Academic Editors: Stéphanie Lambert and Julien Mahy

Received: 17 December 2021

Accepted: 7 January 2022

Published: 19 January 2022

Publisher's Note: MDPI stays neutral with regard to jurisdictional claims in published maps and institutional affiliations.



Copyright: © 2022 by the authors. Licensee MDPI, Basel, Switzerland. This article is an open access article distributed under the terms and conditions of the Creative Commons Attribution (CC BY) license (<https://creativecommons.org/licenses/by/4.0/>).

1. Introduction

The intensive use of drugs for the treatment of human health and industrial wastewater disposal are potential sources of contamination of aqueous effluents [1–4]. Currently, water treatment plants are not designed for the remediation of pharmaceutical and personal care products (PPCPs) [1,2]. An example of PPCPs is the antibiotic tetracycline, used to prevent bacterial infections, found in sewage from the pharmaceutical industry, hospitals, and livestock [5,6]. The remediation of organic compounds, such as chlorophenol, is a priority due to its high toxicity, low biodegradability, and carcinogenic and endocrine disruptive properties [4,7].

In this context, photocatalysis (an advanced oxidative process) is an alternative and sustainable technology for the remediation of these pollutants. The development of new photocatalysts mainly seeks to increase the capacity of the absorption of sunlight, i.e., to expand absorption from the ultra-violet (UV) region to the visible spectrum, since the

visible region comprises ~45% of the solar spectrum [6,8–12]. In addition, the maximization of the photogeneration of reactive oxygen species (ROS), such as $\bullet\text{O}_2^-$ and $\bullet\text{OH}$, plays a key role in photocatalytic activity [13,14]. This maximization occurs through the increase in the formation of e^-/h^+ pairs and, consequently, their interaction with the O_2 and H_2O molecules to generate $\bullet\text{O}_2^-$ and $\bullet\text{OH}$, respectively.

Thus, the visible light sensitization mechanism denominated as the ligand-to-metal charge transfer (LMCT) has gained recognition in the development of TiO_2 -based nano-materials [15], although the effect of point defects should also be considered [16–18]. The LMCT mechanism promotes, in theory, the efficient photogeneration of superoxide radicals under visible light [16] and consists of the direct injection of e^- from the highest occupied molecular orbital (HOMO) of a chelating ligand into the conduction band (CB) of a semiconductor, such as TiO_2 [19]. The LMCT mechanism occurs via bonds formed between the chelating ligands (small organic molecules) and the TiO_2 surface [15,16,19].

The LMCT complex based on TiO_2 and acetic acid (monodentate ligand) showed photodegradation of phenol higher than 90% after 1.5 h exposure to a blue light-emitting diode (LED) lamp (20 W) [20]. In addition, another LMCT complex, made of TiO_2 and salicylic acid (bidentate ligand), revealed the potential for the selective aerobic oxidation of amines to imines under blue LED irradiation (3 W), having a selective yield of 92% of the desired product, N-benzylidenebenzylamine [21]. Other LMCT complexes of TiO_2 and bidentate ligands, such as glucose [22] and alizarin [23], showed ~100% photocatalytic reduction of Cr (VI) during 1 h under visible light irradiation (Xenon lamp 300 W). Furthermore, the nanocrystalline charge transfer complex (CTC) between TiO_2 and acetylacetone (bidentate) calcinated at 300 °C in air revealed ~100% NO_x gas photodegradation for 2 h under visible light irradiation (24 W) [16]. Another study on the amorphous TiO_2 -Acetylacetone complex revealed ~90% degradation of 2,4-dichlorophenol after 24 h in the absence of irradiation in the presence of high catalyst concentration ($1 \text{ g}\cdot\text{L}^{-1}$) [24]. However, as the authors are aware, a CTC such as TiO_2 -bidentate has not been investigated thus far for photocatalytic applications in drug degradation.

Moreover, the understanding of the role of reactive radicals on the photocatalytic activity of these complexes is not fully understood. Experimental analyses performed by electron paramagnetic resonance (EPR) [16,25] and theoretical studies based on density functional theory (DFT) reported for the TiO_2 -Acetylacetone [25] and TiO_2 -Thiosalicylic acid [26] complexes demonstrate the capacity of the LMCT mechanism to produce superoxide ($\bullet\text{O}_2^-$). On the other hand, Fourier transform infrared (FTIR) analysis reveals the presence of adsorbed hydroxyls on the surface of these LMCT complexes [16,20–22,25] that may participate in the formation of $\bullet\text{OH}$ if electronic holes exist in the valence band (VB) of TiO_2 . However, to the best of our knowledge, the individual potential of ROS in the LMCT systems has not been evaluated for photocatalytic applications. The ROS scavengers have been, however, already employed to other photocatalysts in photocatalytic measurements in the liquid medium to assess the individual potential of each ROS [4,6,27–30].

The measurements of photocatalytic degradation of chlorophenol and tetracycline by CTC, combined with the use of $\bullet\text{O}_2^-$ and $\bullet\text{OH}$ scavengers, would clarify the actual potential of each ROS in the photocatalytic abatement.

Photocatalytic degradation in a liquid medium under visible light irradiation is mostly carried out with a light power superior to 300 W [30–33]. The high energy consumption of the lamps follows the opposite path to the sustainable nature of photocatalysis. Therefore, a lamp with reduced power such as residential lamps of 26 W will be applied in this research for the degradation of aqueous pollutants.

This study has as the main goals (1) the evaluation of the potential of TiO_2 -Acetylacetone CTC calcinated at 300 °C in air for the photodegradation of chlorophenol and tetracycline under reduced power visible light (26 W) and (2) an understanding of ROS ($\bullet\text{O}_2^-$ and $\bullet\text{OH}$) roles in photocatalysis performed by TiO_2 -Acetylacetone using scavengers, such as benzoquinone and isopropanol. Furthermore, the volatilization profile of TiO_2 -ACAC CTC

was studied up to 550 °C by thermogravimetric analysis coupled with mass spectroscopy (TGA-MS) to confirm the presence of acetylacetone at temperatures above 150 °C.

2. Results

2.1. Evaluation of TiO₂-ACAC CTC Volatilization Profile by TGA-MS

TiO₂-A-RT, TiO₂-ACAC, and TiO₂-A300 were analyzed by TGA-MS to confirm the presence of ACAC above 150 °C through the release of ACAC fragments or the release of the entire ACAC molecule on heating.

The TGA curve of the TiO₂-A-RT sample (Figure 1a) revealed an expressive mass loss of 29.5 wt.% at temperatures below 150 °C due to dehydration of the material. Furthermore, the mass loss between 150 °C and 450 °C is associated with the release of acetylacetone, as documented by TGA-MS results (Figure 1b). The mass loss of organic species between 150 °C and 450 °C was ~15 wt.% and approximately equal to the mass loss of the TiO₂-ACAC xerogel for the same temperature region [16]. The TGA curves of TiO₂-ACAC and TiO₂-A300 and their first derivatives (DTG) (Figure S1, see Supplementary Materials) were in accordance with the results previously reported by Almeida et al. [16].

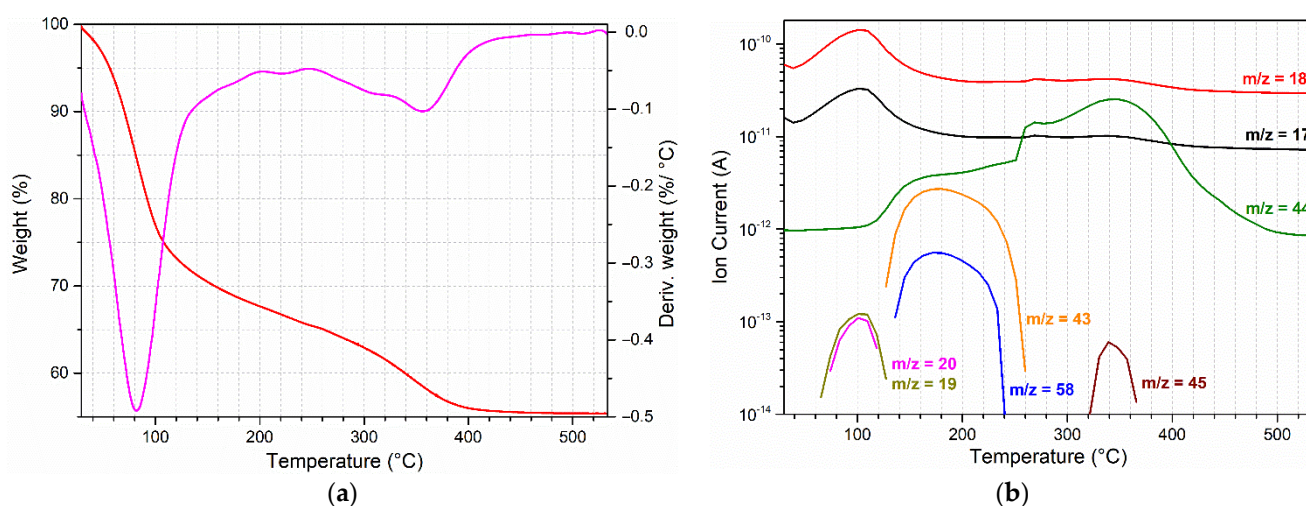


Figure 1. (a) TGA and DTG curves of TiO₂-A-RT sample; (b) Evolution profiles of gaseous species as monitored by TGA-MS for TiO₂-A-RT sample.

Figure 1b illustrates the evolution profiles of released gases as a function of temperature for the TiO₂-A-RT sample. In the first temperature stage of volatilization between 30 °C and 150 °C, species with m/z of 17, 18, 19, and 20, corresponding to water were detected [34]. In the second temperature stage between 150 °C and ~265 °C, the m/z of 43, 44, and 58 were identified, owing to the release of acetyl ions (CH₃C≡O⁺), CO₂, and acetone, respectively [35]. Bowie et al. [35] showed that m/z of 43 and 58 are associated with the fragmentation of the ACAC molecule, where the most intense peak of the ACAC volatilization in the mass spectrum is m/z 43, belonging to acetyl ions. Acetone and CO₂ release in this temperature range are in accordance with Acik et al. [36] who observed the release of both species from the amorphous TiO₂-ACAC xerogel. In the third temperature region of mass loss between 300 °C and 450 °C, an increase of CO₂ release was identified (m/z = 44 and 45) together with water release, which is in accordance with the observation of Acik et al. [36] and Madarász et al. [37] for amorphous TiO₂-ACAC xerogel and crystalline titanium oxobis(acetylacetonate), respectively.

The profiles of gaseous species released from nanocrystalline TiO₂-ACAC and TiO₂-A300 samples are shown in Figure 2. The volatilization stages of TiO₂-ACAC (Figure 2a) follow a similar path as TiO₂-A-RT (Figure 1). TiO₂-ACAC water release occurs in the temperature range between 30 °C and 150 °C, followed by a two-stage release of molecules due to ACAC oxidation above 150 °C. In the interval from 150 °C to ~265 °C, only acetyl ions

($m/z = 43$) and CO_2 ($m/z = 44$) were released. In addition, in the third temperature stage (300–450 °C), CO_2 ($m/z = 44$ and 45) and water release were reported. The absence of acetone release in the TiO_2 -ACAC xerogel probably occurred due to overnight drying at 100 °C, reducing the excess ACAC content in the sample.

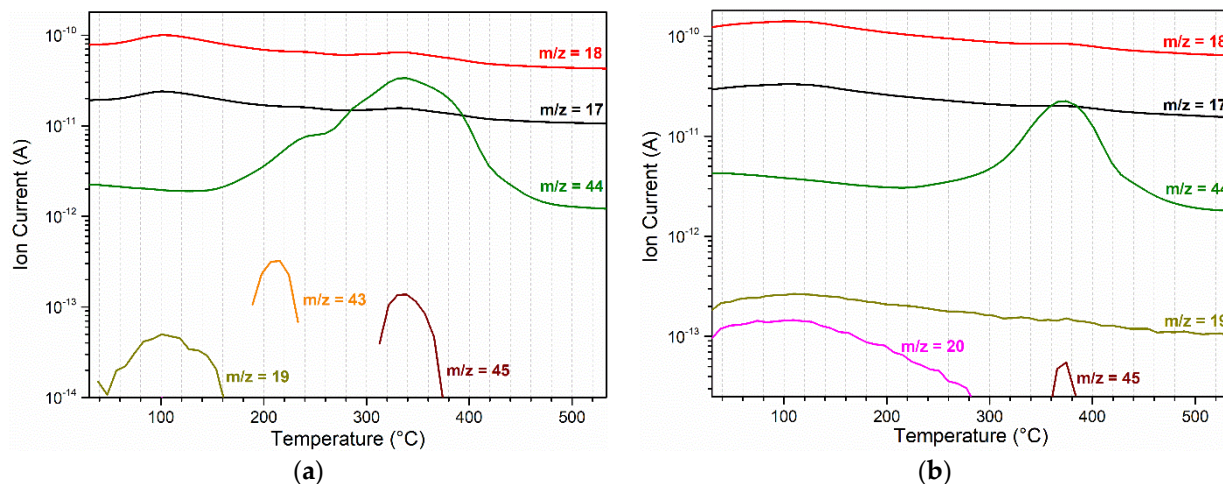


Figure 2. Evolution profiles of gaseous species as monitored by TGA-MS for (a) TiO_2 -ACAC and (b) TiO_2 -A300 samples.

On the other hand, the TGA-MS data of the TiO_2 -A300 sample (Figure 2b) revealed only two distinct temperature stages of gases volatilization. The first stage between 30 °C and 150 °C was related to a release of water ($m/z = 17, 18$ e 19, and 20), while the second stage between 300 °C and 450 °C was due to CO_2 and water release. The volatilization step of the ACAC oxidation products above 300 °C, for all studied TiO_2 -ACAC CTC samples, indirectly contributes to proving that the ACAC is responsible for the sensitization of TiO_2 in visible light in the samples calcined at 300 °C, as previously reported [16].

2.2. Chlorophenol Photodegradation and ROS Efficiency under Reduced Power Visible Light

Figure 3 shows the photocatalytic degradation of chlorophenol using TiO_2 -A300 CTC during the period of 6 h. Photolysis did not promote pollutant degradation (green curve).

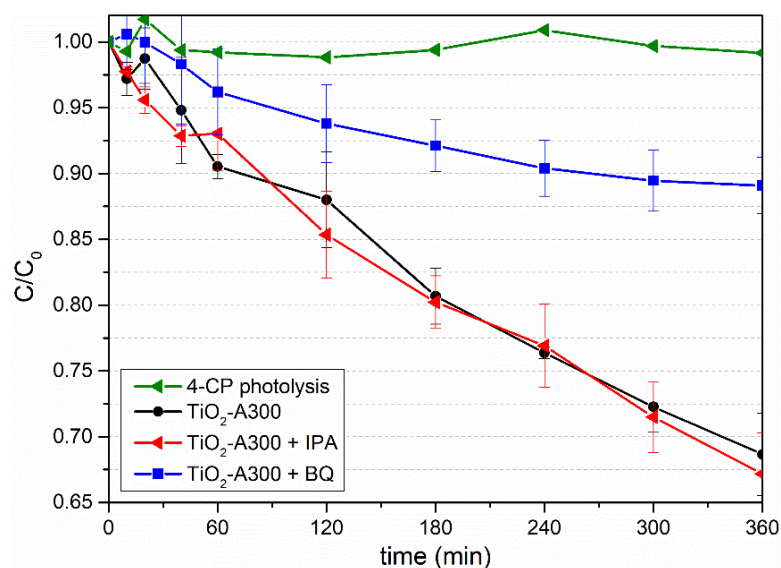


Figure 3. Chlorophenol photodegradation by TiO_2 -A300 photocatalyst with and without the addition of scavengers. The green curve stands for photolysis.

The TiO₂-A300 CTC revealed photocatalytic abatement of 31.3% ± 3.1% for 4-CP after 6 h (Figure 3). Li et al. [32] quantified visible light abatement of 4-CP as 29.9% after 2 h using graphene grafted titania/titanate nanosheets under UV-Vis light of 500 W for the same concentrations of pollutants and photocatalyst used in our study. Furthermore, 4-CP degradation using TiO₂-A300 was nearly half of the degradation reported by Li et al. [32] after 2 h, however, with a light source with 20 times lower power.

The addition of the •OH radical scavenger (IPA) did not significantly impact the degradation efficiency of TiO₂-A300 (Figure 3). The observed photodegradation of 4-CP was 32.8% ± 3.1% after 6 h and was within the error of the degradation measured for TiO₂-A300 without the addition of the IPA scavenger. On the other hand, Moraes et al. [4] revealed that with the addition of the IPA, the degradation of 4-CP (10 mg·L⁻¹) using nanometric anatase (0.2 g·L⁻¹) was about two times lower in comparison to the degradation without the addition of the IPA, however, under UV light and after 3 h. Therefore, these data indicate that hydroxyl radicals played an important role in the degradation of 4-CP for TiO₂ under UV light, since it promoted the formation of e⁻/h⁺ pairs and, consequently, •OH radicals. The results reported by Moraes et al. [4] are in accordance with studies that show that •OH radicals have a dominant role in photodegradation of 4-CP [32,38]. However, for TiO₂-A300 CTC under visible light, it was not possible to detect the role of •OH radicals in the photodegradation of 4-CP. Therefore, our results strongly indicate that TiO₂-A300 CTC does not efficiently generate •OH radicals under visible light.

On the other hand, the addition of the •O₂⁻ scavenger (BQ) caused a strong reduction of the photodegradation potential of TiO₂-A300 (Figure 3). The 4-CP abatement after the addition of BQ was only 10.9% ± 2.1% after 6 h interval. Therefore, the •O₂⁻ plays an important role in the photocatalytic activity of TiO₂-A300 during the degradation of 4-CP. According to Su et al. [39] and Fónagy et al. [40], benzoquinone is predominantly reduced by •O₂⁻ radicals and e⁻ and, consequently, degraded. Therefore, •O₂⁻ generated by TiO₂-A300 CTC preferentially degrades BQ molecules instead of degrading 4-CP, as illustrated in Figure 4. The expressive 76.7% ± 2.1% BQ degradation and low 4-CP degradation after 6 h demonstrate the efficient generation of •O₂⁻ radicals under visible light from TiO₂-A300.

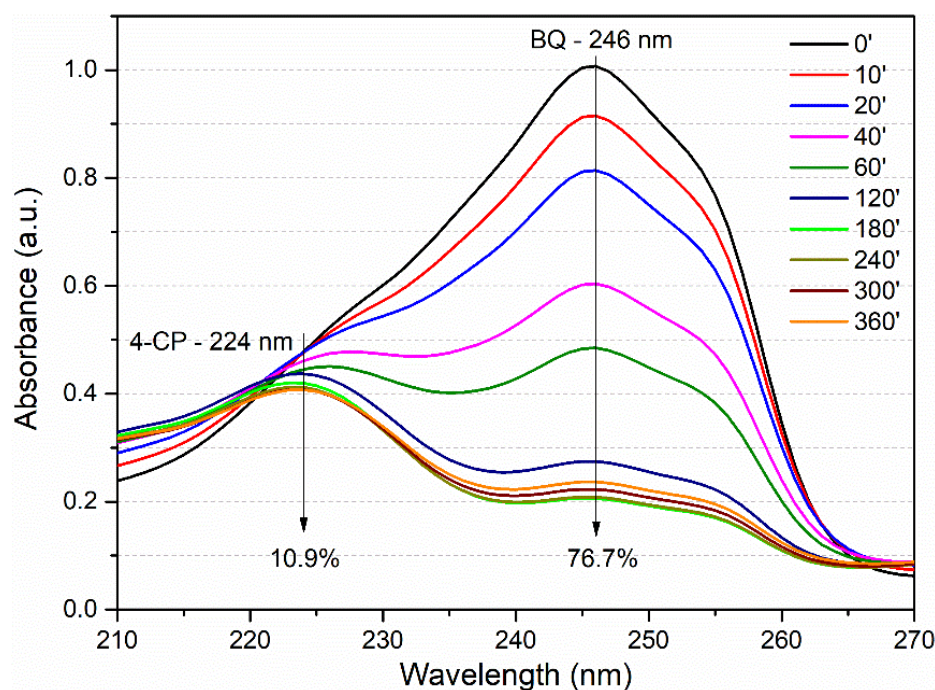


Figure 4. The absorbance of the BQ band situated at 246 nm and the 4-CP band at 224 nm, over time.

2.3. Tetracycline Photodegradation and ROS Efficiency under Reduced Power Visible Light

Figure 5 shows the photocatalytic degradation of tetracycline using TiO₂-A300. The photolysis (green curve) did not show pollutant degradation during the test time.

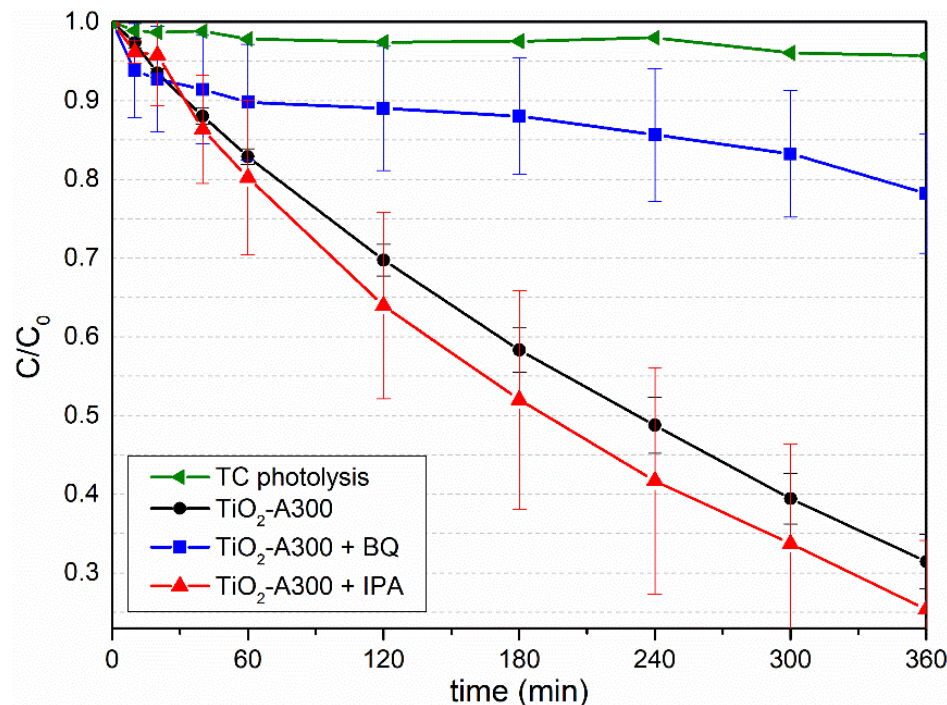


Figure 5. Tetracycline photodegradation by TiO₂-A300 with and without the addition of scavengers. The green curve stands for photolysis.

The TiO₂-A300 CTC showed a high photocatalytic degradation of 68.6% ± 3.4% of TC after 6 h (Figure 5). In addition, the maximum photodegradation of TC up to the abatement stabilization was 83% after 11 h (Figure S2). This maximum abatement of TC from TiO₂-A300 was similar to the 86.7% degradation reported by Wang et al. [6] for the WO₃-TiO₂ core-shell heterostructure decorated by Pt nanoparticles (0.08 g·L⁻¹) under UV-Vis light at 300 W after 2 h. However, the performance of TiO₂-A300 was achieved with 11.5 times lower light power with the use of visible instead of UV light and without the use of precious metals.

The use of isopropanol as the •OH scavenger revealed an abatement of 74.6% ± 8.7% after 6 h, within the error bars of the degradation without the addition of the IPA scavenger. In contrast, TC degradation under UV-Vis light by heterostructures, such as ZnO/GO/Ag₃PO₄ [41], Ag₃PO₄/AgBr/g-C₃N₄ [42], and Bi₂W₂O₉/g-C₃N₄ [43] revealed a decrease in TC abatement due to the addition of IPA. These results reported for the heterostructures indicate that •OH radicals contribute to the degradation of TC when generated [5]. Therefore, the result obtained for TiO₂-A300 suggests that TiO₂-A300 is not capable of producing •OH under visible light.

The TC photodegradation with the addition of BQ was significantly reduced to 21.8% ± 7.6% using TiO₂-A300 after 6 h (Figure 5). The reduction observed in our study agrees with the literature, where different ceramic heterojunctions showed low TC degradation efficiency with the addition of BQ under high power UV or UV-Vis light sources (>300 W) [6,42,44]. He et al. [5] reported that •O₂⁻ and H₂O₂ radicals are capable of attacking the benzene ring of tetracycline, oxidizing the N-dimethyl group and the -C(O)NH₂ group, suggesting that •O₂⁻ plays an important role in the photodegradation pathway of TC. Therefore, the TC degradation behavior observed in Figure 5 is mainly due to the efficient generation of •O₂⁻ radicals by TiO₂-A300 CTC.

3. Discussion

The TGA-MS results of TiO₂-A-RT, TiO₂-ACAC, and TiO₂-A300 samples evidenced the fragments of ACAC oxidation release, such as acetyl ions, acetone, CO₂, and water between 150 °C and ~265 °C, while only CO₂ and water release were detected at higher temperatures between 300 °C and 450 °C (Figures 1b and 2). Two distinct steps of ACAC fragments release for TiO₂-A-RT and TiO₂-ACAC, between 150 °C and 450 °C, are in accordance with the TGA-MS and FTIR-MS analysis reported by Acik et al. [36] for amorphous TiO₂-ACAC xerogel. The volatilization profile of ACAC from TiO₂-A300 (Figure 2b) converges well with the mass loss reported by Almeida et al. [16] for the same material since CO₂ and water were released as ACAC oxidation products above 300 °C. Therefore, it is worth noting for the understanding of the CTC mechanism that nanocrystalline TiO₂-ACAC samples preserved a part of ACAC when calcined at temperatures higher than 150 °C, such as 300 °C, as applied for TiO₂-A300.

The results on the photocatalytic activity of TiO₂-A300 support the hypothesis that a TiO₂-ACAC CTC would be able to degrade aqueous pollutants under reduced power visible light. The TiO₂-A300 showed photocatalytic potential for degradation of both aqueous pollutants 4-CP and TC. In addition, TiO₂-A300 did not show adsorption of pollutants in the dark 1 h before turning on visible light (Figure S3). Therefore, the abatement of all the pollutants was the result of the photocatalytic activity of TiO₂-ACAC CTC.

In our previous study [16], TiO₂-A300 revealed a high efficiency (~100%) for photodegradation of NO_x gas (100 ppm) during 2 h under reduced power visible light (24 W). Therefore, the results presented in the current research additionally increase the photocatalytic applicability of TiO₂-ACAC CTC.

Zhu et al. [41] reported 96.3% degradation of TC (30 mg·L⁻¹) after 75 min, with ~50% of the reported degradation values associated with the adsorption phenomenon in the dark. The authors used for this purpose ZnO/GO/Ag₃PO₄ photocatalyst (1 g·L⁻¹) under low power visible light (65 W). Therefore, photodegradation of TC reported in our study after 6 h (68.6%) was higher than documented by Zhu et al. (46.3%) [41] with 2.5 lower visible light power and using four times less photocatalyst. Additionally, the capacity of degradation of TC is ~two times higher than that observed for 4-CP using TiO₂-A300, after 6 h, indicating a distinct participation of ROS in the degradation of these two pollutants.

ROS Generation Efficiency in TiO₂-A300 CTC

One of the main goals of our study was understanding the roles of ROS ($\bullet\text{O}_2^-$ and $\bullet\text{OH}$) in photocatalysis performed by TiO₂-A300 CTC, using BQ and IPA scavengers. The photodegradation of 4-CP and TC under visible light with the addition of $\bullet\text{O}_2^-$ scavenger confirms the efficient generation of $\bullet\text{O}_2^-$ radicals by TiO₂-ACAC CTC (Figures 3 and 5), in accordance with the EPR characterization and DFT studies carried out on LMCT complexes [16,25,26]. On the other hand, the $\bullet\text{OH}$ radicals were not efficiently generated by TiO₂-A300 CTC under visible light, resulting in the lower photodegradation of 4-CP than the photodegradation of TC, since $\bullet\text{OH}$ radicals are the dominant ROS in the 4-CP photodegradation [4,7,32], while $\bullet\text{O}_2^-$ radicals play a key role in TC degradation [5].

Figure 6 represents an update of the photocatalytic reactions conducted by TiO₂-A300 CTC for the ROS generation and consequent degradation of 4-CP and TC. Additionally, the photocatalytic reactions for hydrogen production are also presented in Figure 6.

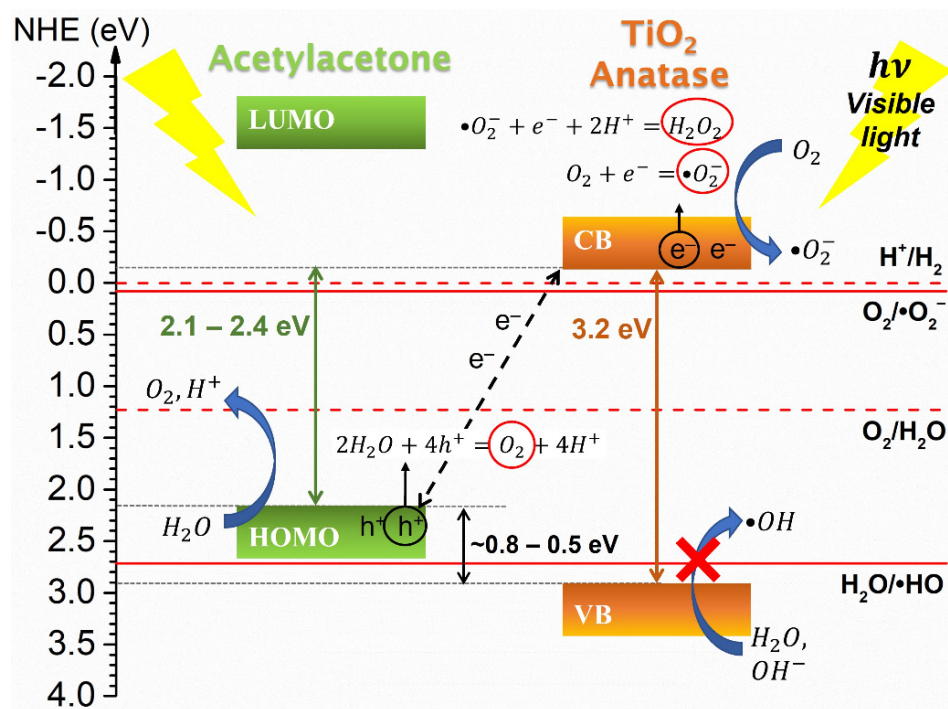


Figure 6. Scheme of electronic bands in TiO₂-A300 CTC and photocatalytic reactions for ROS generation. The position of BV and BC of anatase at redox potential scale, in accordance with normal hydrogen electrode (NHE), was adopted from literature [8,9], as well as the positions of the ROS species. The position of HOMO of acetylacetone was previously established in [16]. The position of LUMO of acetylacetone was arbitrarily added, since it does not have a role in photocatalytic and water splitting events and is higher than 3.2 eV.

Figure 6 shows the electron transfer from ACAC HOMO to TiO₂ (anatase) CB and, consequently, the formation of $\bullet\text{O}_2^-$ radicals due to the reaction between O₂ adsorbed on the surface of anatase and free e⁻ from CB (Equation (1)).



The efficient $\bullet\text{O}_2^-$ generation is also a consequence of a high O₂ presence in the reaction medium [9]. A possible additional explanation for the O₂ presence in an aqueous solution is the water splitting mechanism (Equation (2)) [8,9]. The h⁺ generated in the HOMO of the ACAC may promote water splitting, i.e., decomposing H₂O into O₂ and H⁺ through an oxidation half reaction as shown in Figure 6.



Additionally, the efficient production of $\bullet\text{O}_2^-$ radicals can also form H₂O₂ [9,45], which is another ROS capable of degradation of aqueous pollutants due to its ability to attack benzene rings and the N-dimethyl group [5]. The energy barrier of the formation of H₂O₂ from $\bullet\text{O}_2^-$ radicals (Equation (3)) is 0.3 eV below the normal hydrogen electrode potential (NHE) [13]. Therefore, a part of $\bullet\text{O}_2^-$ generated by TiO₂-A300 can be transformed into H₂O₂ and can continue to degrade 4-CP and TC.



As seen in Figure 6, the arrangement of CB of TiO₂ and HOMO of ACAC in the TiO₂-ACAC CTC may provide photocatalytic production of H₂ from water splitting. The electron

holes from HOMO of ACAC are capable of oxidizing water, forming H^+ (Equation (2)), and the e^- in the CB of TiO_2 may reduce H^+ to H_2 (Equation (4)).



Finally, some previous studies demonstrated the photocatalytic potential of Z-scheme heterostructures based on WO_3 [6,46], SnO_2 [47], and $BiVO_4$ [48] for TC and NO_x degradation and hydrogen production under UV-Vis light. These low-bandgap semiconductors can absorb visible light and generate $\bullet OH$ radicals via VB and CB with positive redox potential. The Z-scheme heterojunction consists of the recombination of the CB electrons of these low-bandgap semiconductors with the VB of another semiconductor with a lower positive redox potential, providing a reduction in the recombination rate of e^-/h^+ pairs in the low-bandgap semiconductors, such as WO_3 , SnO_2 , and $BiVO_4$ and, consequently, an increase in the formation of $\bullet OH$ radicals. Therefore, coupling TiO_2 -ACAC CTC with semiconductors capable of generating $\bullet OH$ radicals under visible light may maximize the generation of ROS and increase of photocatalytic efficiency of these new heterojunctions.

4. Materials and Methods

4.1. Materials

All reagents were purchased from Sigma-Aldrich and used as obtained. Titanium isopropoxide ($Ti(OiPr)_4$, 97%), acetylacetone (ACAC, $\geq 99\%$), ethanol ($\geq 99.8\%$), and nitric acid (65%) were used for the synthesis of TiO_2 -ACAC CTC nanoparticles. The aqueous pollutants were chlorophenol (4-CP, $\geq 99\%$) and tetracycline (TC, $\geq 98\%$). Benzoquinone (BQ, $\geq 98\%$) and isopropanol (IPA, $\geq 99.5\%$) were used as ROS scavengers.

4.2. Synthesis of TiO_2 -Acetylacetone Charge Transfer Complex

The synthesis of TiO_2 anatase nanoparticles coupled with acetylacetone (CTC) was carried out by the sol-gel route as reported by Scolan and Sanchez [49]. In addition, as previously reported [12,16], the molar ratios for hydrolysis ($H = [H_2O]/[Ti]$), acidity ($H^+ = [H^+]/[Ti]$), and complexing ($A = [ACAC]/[Ti]$) were kept at 100, 0.027 and 2, respectively, to produce TiO_2 -ACAC xerogel with mean crystal size ~ 2.5 nm.

In the adopted procedure, 30 mL of $Ti(OiPr)_4$ was added dropwise into a solution of 20 mL of ACAC with 100 mL of ethanol (1:5 *v/v*). The obtained yellow solution remained under magnetic stirring for 40 min at room temperature. Afterward, 180 mL of HNO_3 solution (0.015 M) was dropped slowly into the yellowish solution under continuous stirring. The dark orange solution obtained was heated to 60 °C and kept under magnetic stirring for 8 h. Next, the sol of TiO_2 was dried overnight in Petri dishes at room temperature, and a gel was formed (TiO_2 -A-RT). Finally, the gel was dried at 100 °C overnight to obtain a red-yellowish xerogel of TiO_2 -Acetylacetone (TiO_2 -ACAC). The TiO_2 -ACAC xerogel, grounded in an agate mortar, was calcined in air at 300 °C for 2 h in a Tubular Maitec-INTI FET 1600/H furnace. The as-prepared powder was denoted TiO_2 -A300.

4.3. Thermogravimetric Analysis Coupled with Mass Spectroscopy (TGA-MS)

Thermogravimetric analysis (TGA) and differential scanning calorimetry (DSC) were performed on a Perkin-Elmer Simultaneous Thermal Analyzer STA-6000 under synthetic air flow ($130 \text{ mL}\cdot\text{min}^{-1}$) with a heating rate of $10 \text{ }^\circ\text{C}\cdot\text{min}^{-1}$ and within the temperature range between 30 °C and 550 °C. A mass of ~ 25 mg was used.

To identify the volatilized species from TiO_2 -ACAC and confirm the presence of ACAC in the TiO_2 -A300 sample, a mass spectrometer OmniStar/ThermoStar-GSD 320 O3 (Pfeiffer Vacuum) was coupled to the STA-6000. The *m/z* range until 105 was scanned with the measuring time of $0.5 \text{ s}\cdot\text{amu}^{-1}$.

4.4. Measurement of the Photodegradation of Chlorophenol and Tetracycline and the Efficiency of ROS

The photocatalytic potential of TiO₂-A300 for degradation of 5 mg·L⁻¹ of 4-CP and TC under visible light irradiation was evaluated. In accordance with [16], the inorganic part of TiO₂-A300 CTC is composed of nanocrystalline anatase. Two other materials, TiO₂-A-RT and TiO₂-ACAC (where the inorganic part also consists of nanocrystalline anatase), were not evaluated since they previously showed inferior photocatalytic efficiency [16]. In addition, a measurement of the TC photodegradation until stabilization of TC abatement was performed.

All measurements were performed with 0.2 g·L⁻¹ of the photocatalyst. The light source used was a DULUX D/E 26 W residential fluorescent lamp with an irradiance of 0.23 W·cm⁻² and an emission of light in the wavelength range from 400 nm to 700 nm. The photocatalytic system is shown in Figure S4. The lamp is housed in a cylindrical quartz bulb (length 11 cm, internal diameter 3.2 cm, and thickness 0.15 cm) unable to absorb visible light. The photoreactor was immersed in a bath with cold water circulation to maintain the system at room temperature. The photocatalytic tests were carried out under vigorous magnetic stirring in two stages. In the first stage, the pollutant and the photocatalyst were kept in the dark for 1 h to attain the absorption–desorption equilibrium. After this period, the lamp was turned on, and 5 mL aliquots of supernatant were acquired at intervals of 1 h for 6 h. The supernatant was filtered through a Merck Millipore filter (0.45 µm) and analyzed by an Agilent UV-Vis spectrophotometer (model 8453). The absorption at the wavelengths of 224 nm and 358 nm was accompanied for photodegradation of 4-CP and TC during the test time, respectively. The observed reduction in these wavelengths for each pollutant was used as input to determine the percentage of photodegradation performed by TiO₂-A300 CTC, as seen in Figure S5 and Table S1. The degradation data obtained were presented through the mean value together with the respective standard deviations (Table S1) since all photocatalytic tests were performed in triplicate to ensure repeatability of results.

The ROS efficiency in TiO₂-ACAC CTC was evaluated by adding the scavenger molecule BQ (5.4 mg·L⁻¹; 0.05 mmol·L⁻¹) to inhibit the participation of the •O₂⁻ radical in the degradation of 4-CP and TC. On the other hand, the addition of the IPA scavenger (6.0 mg·L⁻¹; 0.1 mmol·L⁻¹) was performed to inhibit the participation of the •OH radical. The scavengers were added to the 5.0 mg·L⁻¹ solutions of 4-CP or TC before starting the photocatalytic tests to ensure a mass ratio close to 1:1 between the pollutant and the scavenger.

5. Conclusions

The TGA-MS indirectly proved the presence of ACAC on TiO₂-A-RT, TiO₂-ACAC xerogel, and TiO₂-A300 at temperatures higher than 150 °C. The release of acetyl ions and acetone between 150 °C and ~265 °C was detected, while at temperatures above 300 °C, and not higher than 450 °C, the release of CO₂ and water was detected as the products of ACAC oxidation.

The TiO₂-A300 photodegrades 4-CP and TC under reduced power visible light. The photocatalytic abatement of tetracycline (68.6%) was ~two times higher than that observed for chlorophenol (31.3%) after 6 h, indicating a distinct potential of ROS in the degradation of these pollutants.

The addition of BQ scavenger on the photocatalytic degradation of 4-CP and TC proved TiO₂-A300 CTC to be a powerful source of superoxide (•O₂⁻) radicals under visible light, promoting a high photodegradation of TC (68.6%) after 6 h. However, the •OH scavenger does not promote the reduction in photodegradation of 4-CP and TC, proving TiO₂-ACAC CTC is not an efficient generator of •OH radicals under visible light.

The photocatalytic potential reported for TiO₂-A300 may stimulate new studies on hydrogen production process from water splitting under visible light due to the redox potential arrangement of CB of TiO₂ and HOMO of ACAC. Furthermore, the development

of heterostructures based on TiO₂-A300 CTC, and similar CTC, can increase the generation of ROS through coupling with semiconductors capable of generating •OH under visible light and, therefore, capable of formation of more powerful photocatalysts.

Supplementary Materials: The following are available online at <https://www.mdpi.com/article/10.3390/catal12020116/s1>, Figure S1: TGA and DTG curves of (a) TiO₂-ACAC xerogel and (b) TiO₂-A300 sample, Figure S2: Tetracycline photodegradation by TiO₂-A300, Figure S3: Curves of adsorption (1 h in dark) and photocatalytic activity of 4-CP and TC using TiO₂-A300 of (a) 4-CP and (b) TC by TiO₂-A300 without scavengers addition during 6 h, Figure S4: Photocatalytic system for aqueous pollutants degradation, Figure S5: Absorbance of (a) 4-CP band, situated at 224 nm and (b) TC band at 358 nm, over the time, Table S1: 4-CP and TC degradation data obtained in the first repetition of the photocatalytic test using TiO₂-A300.

Author Contributions: Conceptualization, L.A.A. and B.A.M.; synthesis and overall characterizations, L.A.A.; funding acquisition, B.A.M.; data interpretation, L.A.A. and B.A.M.; TGA-MS analysis, A.D. and J.V.; TGA-MS interpretation, A.D. and J.V.; writing—original draft preparation, L.A.A.; writing—review and editing, L.A.A., A.D. and B.A.M. All authors have read and agreed to the published version of the manuscript.

Funding: The authors are grateful to FAPERJ for financial support through the projects E-26/210.585/2019 and E-26/210.046/2021.

Institutional Review Board Statement: Not applicable.

Informed Consent Statement: Not applicable.

Data Availability Statement: The data underlying this article will be shared on reasonable request from the corresponding author.

Acknowledgments: This study was financed in part by the Coordenação de Aperfeiçoamento de Pessoal de Nível Superior-Brasil (CAPES)—Finance Code 001. B.A.M. is grateful to CNPq (National Council for Scientific and Technological Development) for a Research Productivity Grant. L.A. is grateful to ANP (Agência Nacional do Petróleo, Gás Natural e Biocombustíveis) and Finep (Funding Authority for Studies and Projects) for a doctoral degree scholarship.

Conflicts of Interest: The authors declare no conflict of interest.

References

1. Liu, N.; Wang, J.; Wu, J.; Li, Z.; Huang, W.; Zheng, Y.; Lei, J.; Zhang, X.; Tang, L. Magnetic Fe₃O₄@MIL-53(Fe) nanocomposites derived from MIL-53(Fe) for the photocatalytic degradation of ibuprofen under visible light irradiation. *Mater. Res. Bull.* **2020**, *132*, 111000. [[CrossRef](#)]
2. Zhou, Z.; Li, Y.; Li, M.; Li, Y.; Zhan, S. Efficient removal for multiple pollutants via Ag₂O/BiOBr heterojunction: A promoted photocatalytic process by valid electron transfer pathway. *Chin. Chem. Lett.* **2020**, *31*, 2698–2704. [[CrossRef](#)]
3. Mohammad, A.; Khan, M.E.; Cho, M.H.; Yoon, T. Adsorption promoted visible-light-induced photocatalytic degradation of antibiotic tetracycline by tin oxide/cerium oxide nanocomposite. *Appl. Surf. Sci.* **2021**, *565*, 150337. [[CrossRef](#)]
4. de Moraes, N.P.; Torezin, F.A.; Dantas, G.V.J.; de Sousa, J.G.M.; Valim, R.B.; da Silva Rocha, R.; Landers, R.; da Silva, M.L.C.P.; Rodrigues, L.A. TiO₂/Nb₂O₅/carbon xerogel ternary photocatalyst for efficient degradation of 4-Chlorophenol under solar light irradiation. *Ceram. Int.* **2020**, *46*, 14505–14515. [[CrossRef](#)]
5. He, X.; Kai, T.; Ding, P. Heterojunction photocatalysts for degradation of the tetracycline antibiotic: A review. *Environ. Chem. Lett.* **2021**, *19*, 4563–4601. [[CrossRef](#)]
6. Wang, Y.; Fu, H.; Yang, X.; An, X.; Zou, Q.; Xiong, S.; Han, D. Pt nanoparticles-modified WO₃@TiO₂ core-shell ternary nanocomposites as stable and efficient photocatalysts in tetracycline degradation. *J. Mater. Sci.* **2020**, *55*, 14415–14430. [[CrossRef](#)]
7. de Moraes, N.P.; Valim, R.B.; da Silva Rocha, R.; da Silva, M.L.C.P.; Campos, T.M.B.; Thim, G.P.; Rodrigues, L.A. Effect of synthesis medium on structural and photocatalytic properties of ZnO/Carbon xerogel composites for solar and visible light degradation of 4-Chlorophenol and bisphenol A. *Colloids Surf. A Physicochem. Eng. Asp.* **2020**, *584*, 124034. [[CrossRef](#)]
8. Christoforidis, K.C.; Fornasiero, P. Photocatalytic Hydrogen Production: A Rift into the Future Energy Supply. *ChemCatChem* **2017**, *9*, 1523–1544. [[CrossRef](#)]
9. Ren, H.; Koshy, P.; Chen, W.-F.; Qi, S.; Sorrell, C.C. Photocatalytic materials and technologies for air purification. *J. Hazard. Mater.* **2017**, *325*, 340–366. [[CrossRef](#)]
10. Kapilashrami, M.; Zhang, Y.; Liu, Y.-S.; Hagfeldt, A.; Guo, J. Probing the Optical Property and Electronic Structure of TiO₂ Nanomaterials for Renewable Energy Applications. *Chem. Rev.* **2014**, *114*, 9662–9707. [[CrossRef](#)] [[PubMed](#)]

11. Zhou, H.; Qu, Y.; Zeid, T.; Duan, X. Towards highly efficient photocatalysts using semiconductor nanoarchitectures. *Energy Environ. Sci.* **2012**, *5*, 6732–6743. [[CrossRef](#)]
12. Habran, M.; Pontón, P.I.; Mancic, L.; Pandoli, O.; Krambrock, K.; da Costa, M.E.H.M.; Letichevsky, S.; Costa, A.M.L.M.; Morgado, E.; Marinkovic, B.A. Visible light sensitive mesoporous nanohybrids of lepidocrocite-like ferrititanate coupled to a charge transfer complex: Synthesis, characterization and photocatalytic degradation of NO. *J. Photochem. Photobiol. A Chem.* **2018**, *365*, 133–144. [[CrossRef](#)]
13. Nosaka, Y.; Nosaka, A.Y. Generation and Detection of Reactive Oxygen Species in Photocatalysis. *Chem. Rev.* **2017**, *117*, 11302–11336. [[CrossRef](#)]
14. Khavar, A.H.C.; Moussavi, G.; Mahjoub, A.R.; Luque, R.; Rodríguez-Padrón, D.; Sattari, M. Enhanced visible light photocatalytic degradation of acetaminophen with Ag₂S-ZnO@rGO core-shell microsphere as a novel catalyst: Catalyst preparation and characterization and mechanistic catalytic experiments. *Sep. Purif. Technol.* **2019**, *229*, 115803. [[CrossRef](#)]
15. Luciani, G.; Imparato, C.; Vitiello, G. Photosensitive Hybrid Nanostructured Materials: The Big Challenges for Sunlight Capture. *Catalysts* **2020**, *10*, 103. [[CrossRef](#)]
16. Almeida, L.A.; Habran, M.; dos Santos Carvalho, R.; da Costa, M.E.H.M.; Cremona, M.; Silva, B.C.; Krambrock, K.; Pandoli, O.G.; Morgado, E., Jr.; Marinkovic, B.A. The Influence of Calcination Temperature on Photocatalytic Activity of TiO₂-Acetylacetone Charge Transfer Complex towards Degradation of NO_x under Visible Light. *Catalysts* **2020**, *10*, 1463. [[CrossRef](#)]
17. Piskunov, S.; Lisovski, O.; Begens, J.; Bocharov, D.; Zhukovskii, Y.F.; Wessel, M.; Spohr, E. C-, N-, S-, and Fe-Doped TiO₂ and SrTiO₃ Nanotubes for Visible-Light-Driven Photocatalytic Water Splitting: Prediction from First Principles. *J. Phys. Chem. C* **2015**, *119*, 18686–18696. [[CrossRef](#)]
18. Serga, V.; Burve, R.; Krumina, A.; Pankratova, V.; Popov, A.I.; Pankratov, V. Study of phase composition, photocatalytic activity, and photoluminescence of TiO₂ with Eu additive produced by the extraction-pyrolytic method. *J. Mater. Res. Technol.* **2021**, *13*, 2350–2360. [[CrossRef](#)]
19. Zhang, G.; Kim, G.; Choi, W. Visible light driven photocatalysis mediated via ligand-to-metal charge transfer (LMCT): An alternative approach to solar activation of titania. *Energy Environ. Sci.* **2014**, *7*, 954–966. [[CrossRef](#)]
20. Liu, J.; Han, L.; An, N.; Xing, L.; Ma, H.; Cheng, L.; Yang, J.; Zhang, Q. Enhanced visible-light photocatalytic activity of carbonate-doped anatase TiO₂ based on the electron-withdrawing bidentate carboxylate linkage. *Appl. Catal. B Environ.* **2017**, *202*, 642–652. [[CrossRef](#)]
21. Li, X.; Xu, H.; Shi, J.-L.; Hao, H.; Yuan, H.; Lang, X. Salicylic acid complexed with TiO₂ for visible light-driven selective oxidation of amines into imines with air. *Appl. Catal. B Environ.* **2019**, *244*, 758–766. [[CrossRef](#)]
22. Kim, G.; Lee, S.-H.; Choi, W. Glucose-TiO₂ charge transfer complex-mediated photocatalysis under visible light. *Appl. Catal. B Environ.* **2015**, *162*, 463–469. [[CrossRef](#)]
23. Li, M.; Li, Y.; Zhao, J.; Li, M.; Wu, Y.; Na, P. Alizarin-TiO₂ LMCT Complex with Oxygen Vacancies: An Efficient Visible Light Photocatalyst for Cr(VI) Reduction. *Chin. J. Chem.* **2020**, *38*, 1332–1338. [[CrossRef](#)]
24. Aronne, A.; Fantauzzi, M.; Imparato, C.; Atzei, D.; De Stefano, L.; D'Errico, G.; Sannino, F.; Rea, I.; Pirozzi, D.; Elsener, B.; et al. Electronic properties of TiO₂-based materials characterized by high Ti₃⁺ self-doping and low recombination rate of electron-hole pairs. *RSC Adv.* **2017**, *7*, 2373–2381. [[CrossRef](#)]
25. Ritacco, I.; Imparato, C.; Falivene, L.; Cavallo, L.; Magistrato, A.; Caporaso, L.; Camellone, M.F.; Aronne, A. Spontaneous Production of Ultrastable Reactive Oxygen Species on Titanium Oxide Surfaces Modified with Organic Ligands. *Adv. Mater. Interfaces* **2021**, *8*, 2100629. [[CrossRef](#)]
26. Miličević, B.; Đorđević, V.; Lončarević, D.; Dostanić, J.M.; Ahrenkiel, S.P.; Dramićanin, M.D.; Sredojević, D.; Švrakić, N.M.; Nedeljković, J.M. Charge-transfer complex formation between TiO₂ nanoparticles and thiosalicylic acid: A comprehensive experimental and DFT study. *Opt. Mater.* **2017**, *73*, 163–171. [[CrossRef](#)]
27. Lam, S.M.; Sin, J.-C.; Satoshi, I.; Abdullah, A.Z.; Mohamed, A.R. Enhanced sunlight photocatalytic performance over Nb₂O₅/ZnO nanorod composites and the mechanism study. *Appl. Catal. A Gen.* **2014**, *471*, 126–135. [[CrossRef](#)]
28. Abd Elkodous, M.; El-Sayyad, G.S.; Abdel Maksoud, M.I.A.; Kumar, R.; Maegawa, K.; Kawamura, G.; Tan, W.K.; Matsuda, A. Nanocomposite matrix conjugated with carbon nanomaterials for photocatalytic wastewater treatment. *J. Hazard. Mater.* **2021**, *410*, 124657. [[CrossRef](#)]
29. Zhang, Y.; Li, J.; Liu, H. Synergistic Removal of Bromate and Ibuprofen by Graphene Oxide and TiO₂ Heterostructure Doped with F: Performance and Mechanism. *J. Nanomater.* **2020**, *2020*, 6094984. [[CrossRef](#)]
30. de Sousa, J.G.M.; da Silva, T.V.C.; de Moraes, N.P.; da Silva, M.L.C.P.; da Silva Rocha, R.; Landers, R.; Rodrigues, L.A. Visible light-driven ZnO/g-C₃N₄/carbon xerogel ternary photocatalyst with enhanced activity for 4-Chlorophenol degradation. *Mater. Chem. Phys.* **2020**, *256*, 123651. [[CrossRef](#)]
31. Myilsamy, M.; Mahalakshmi, M.; Subha, N.; Rajabhuvaneswari, A.; Murugesan, V. Visible light responsive mesoporous graphene-Eu₂O₃/TiO₂ nanocomposites for the efficient photocatalytic degradation of 4-Chlorophenol. *RSC Adv.* **2016**, *6*, 35024–35035. [[CrossRef](#)]
32. Li, F.; Du, P.; Liu, W.; Li, X.; Ji, H.; Duan, J.; Zhao, D. Hydrothermal synthesis of graphene grafted titania/titanate nanosheets for photocatalytic degradation of 4-Chlorophenol: Solar-light-driven photocatalytic activity and computational chemistry analysis. *Chem. Eng. J.* **2018**, *331*, 685–694. [[CrossRef](#)]

33. Alam, U.; Shah, T.A.; Khan, A.; Muneer, M. One-pot ultrasonic assisted sol-gel synthesis of spindle-like Nd and V codoped ZnO for efficient photocatalytic degradation of organic pollutants. *Sep. Purif. Technol.* **2019**, *212*, 427–437. [[CrossRef](#)]
34. Acik, I.O.; Madarász, J.; Krunks, M.; Tönsuaadu, K.; Pokol, G.; Niinistö, L. Titanium(IV) acetylacetonate xerogels for processing titania films: A Thermoanalytical Study. *J. Therm. Anal. Calorim.* **2009**, *97*, 39–45. [[CrossRef](#)]
35. Bowie, J.H.; Williams, D.H.; Lawesson, S.-O.; Schroll, G. Studies in Mass Spectrometry. IX.1 Mass Spectra of β -Diketones. *J. Org. Chem.* **1966**, *31*, 1384–1390. [[CrossRef](#)]
36. Acik, I.O.; Madarász, J.; Krunks, M.; Tönsuaadu, K.; Janke, D.; Pokol, G.; Niinistö, L. Thermoanalytical studies of titanium(IV) acetylacetonate xerogels with emphasis on evolved gas analysis. *J. Therm. Anal. Calorim.* **2007**, *88*, 557–563. [[CrossRef](#)]
37. Madarász, J.; Kaneko, S.; Okuya, M.; Pokol, G. Comparative evolved gas analyses of crystalline and amorphous titanium(IV)oxo-hydroxo-acetylacetonates by TG-FTIR and TG/DTA-MS. *Thermochim. Acta* **2009**, *489*, 37–44. [[CrossRef](#)]
38. Schneider, J.; Matsuoka, M.; Takeuchi, M.; Zhang, J.; Horiuchi, Y.; Anpo, M.; Bahnemann, D.W. Understanding TiO₂ Photocatalysis: Mechanisms and Materials. *Chem. Rev.* **2014**, *114*, 9919–9986. [[CrossRef](#)]
39. Su, R.; Tiruvalam, R.; He, Q.; Dimitratos, N.; Kesavan, L.; Hammond, C.; Lopez-Sanchez, J.A.; Bechstein, R.; Kiely, C.J.; Hutchings, G.J.; et al. Promotion of Phenol Photodecomposition over TiO₂ Using Au, Pd, and Au–Pd Nanoparticles. *ACS Nano* **2012**, *6*, 6284–6292. [[CrossRef](#)] [[PubMed](#)]
40. Fónagy, O.; Szabó-Bárdos, E.; Horváth, O. 1,4-Benzoquinone and 1,4-Hydroquinone based determination of electron and superoxide radical formed in heterogeneous photocatalytic systems. *J. Photochem. Photobiol. A Chem.* **2021**, *407*, 113057. [[CrossRef](#)]
41. Zhu, P.; Duan, M.; Wang, R.; Xu, J.; Zou, P.; Jia, H. Facile synthesis of ZnO/GO/Ag₃PO₄ heterojunction photocatalyst with excellent photodegradation activity for tetracycline hydrochloride under visible light. *Colloids Surf. A Physicochem. Eng. Asp.* **2020**, *602*, 125118. [[CrossRef](#)]
42. Yu, H.; Wang, D.; Zhao, B.; Lu, Y.; Wang, X.; Zhu, S.; Qin, W.; Huo, M. Enhanced photocatalytic degradation of tetracycline under visible light by using a ternary photocatalyst of Ag₃PO₄/AgBr/g-C₃N₄ with dual Z-scheme heterojunction. *Sep. Purif. Technol.* **2020**, *237*, 116365. [[CrossRef](#)]
43. Obregón, S.; Ruíz-Gómez, M.A.; Rodríguez-González, V.; Vázquez, A.; Hernández-Uresti, D.B. A novel type-II Bi₂W₂O₉/g-C₃N₄ heterojunction with enhanced photocatalytic performance under simulated solar irradiation. *Mater. Sci. Semicond. Process.* **2020**, *113*, 105056. [[CrossRef](#)]
44. Lu, F.; Chen, K.; Feng, Q.; Cai, H.; Ma, D.; Wang, D.; Li, X.; Zuo, C.; Wang, S. Insight into the enhanced magnetic separation and photocatalytic activity of Sn-doped TiO₂ core-shell photocatalyst. *J. Environ. Chem. Eng.* **2021**, *9*, 105840. [[CrossRef](#)]
45. Mamaghani, A.H.; Haghighat, F.; Lee, C.-S. Photocatalytic oxidation technology for indoor environment air purification: The state-of-the-art. *Appl. Catal. B Environ.* **2017**, *203*, 247–269. [[CrossRef](#)]
46. Zhi, L.; Zhang, S.; Xu, Y.; Tu, J.; Li, M.; Hu, D.; Liu, J. Controlled growth of AgI nanoparticles on hollow WO₃ hierarchical structures to act as Z-scheme photocatalyst for visible-light photocatalysis. *J. Colloid Interface Sci.* **2020**, *579*, 754–765. [[CrossRef](#)] [[PubMed](#)]
47. Li, Y.; Wu, X.; Ho, W.; Lv, K.; Li, Q.; Li, M.; Lee, S.C. Graphene-induced formation of visible-light-responsive SnO₂-Zn₂SnO₄ Z-scheme photocatalyst with surface vacancy for the enhanced photoreactivity towards NO and acetone oxidation. *Chem. Eng. J.* **2018**, *336*, 200–210. [[CrossRef](#)]
48. Zhou, F.Q.; Fan, J.C.; Xu, Q.J.; Min, Y.L. BiVO₄ nanowires decorated with CdS nanoparticles as Z-scheme photocatalyst with enhanced H₂ generation. *Appl. Catal. B Environ.* **2017**, *201*, 77–83. [[CrossRef](#)]
49. Scolan, E.; Sanchez, C. Synthesis and Characterization of Surface-Protected Nanocrystalline Titania Particles. *Chem. Mater.* **1998**, *10*, 3217–3223. [[CrossRef](#)]